http://dx.doi.org/10.18623/rvd.v22.n2.3223

FIRST-PRINCIPLES STUDY OF THE STRUCTURAL, ELECTRONIC, AND ELASTIC PROPERTIES OF HYDRIDE PEROVSKITES XCAH₃ (X = NA, K, RB,CS) UNDER PRESSURE

ESTUDO DE PRIMEIROS PRINCÍPIOS DAS PROPRIEDADES ESTRUTURAIS, ELETRÔNICAS E ELÁSTICAS DOS PEROVSKITES HIDRETOS XCAH₃ (X = NA, K, RB, CS) SOB PRESSÃO

Article received on: 13/01/2025
Article accepted on: 29/09/2025

Bassoud Ahmed*
*Laboratory of Physical Chemistry of Advanced Materials, University of Djillali Liabes
BP 89, Sidi-Bel-Abbes 22000, Algeria
Sidi Bel-Abbès, Algeria
Orcid: https://orcid.org/0009-0003-3313-5614
ahmedbassoud@yahoo.fr

Ameri Mohamed*
*Laboratory of Physical Chemistry of Advanced Materials, University of Djillali Liabes
BP 89, Sidi-Bel-Abbes 22000, Algeria
Sidi Bel-Abbès, Algeria
Orcid: https://orcid.org/0000-0002-1978-0823
lttnsameri@yahoo.fr

Sehoul Baghdad**
**Laboratory of Electronic Systems, Telecommunications and Renewable Energy, Nour Bachir El-Bayadh University Center, BP 900 route Aflou, 32000 El Bayadh, Algeria
El-Bayadh, Algeria
Orcid: https://orcid.org/0009-0000-2335-2971
baghdad2006@yahoo.fr

Benfrid Abdelmoutalib***
***Institute of Technology, Maghnia University Centre
Maghnia, Algeria
Orcid: https://orcid.org/0009-0007-8171-1654
benfridabdelmoutalib2050@gmail.com

The authors declare that there is no conflict of interest

Abstract
This study is a thorough investigation. It is founded on fundamental ideas. Density functional theory is what we employ. Structural, electronic, and elastic properties of the hydride perovskites $XCaH_3$ (where X = Na, K, Rb, and Cs) have been investigated using DFT. Through energy–volume optimisation, equilibrium Lattice Constants were determined, demonstrating their stability in the cubic perovskite phase. The electronic band structures and density of states of all compounds indicate that they exhibit semiconducting behavior with direct band gaps. The estimated band gap energies are 3.14 eV for $CsCaH_3$, 3.29 eV for $KCaH_3$, 3.35 eV for

Resumo
Este estudo é uma investigação completa. Baseia-se em ideias fundamentais. A teoria do funcional da densidade é o que empregamos. As propriedades estruturais, eletrônicas e elásticas das perovskitas de hidreto $XCaH_3$ (onde X = Na, K, Rb e Cs) foram investigadas usando DFT. Por meio da otimização energia-volume, as constantes de rede de equilíbrio foram determinadas, demonstrando sua estabilidade na fase perovskita cúbica. As estruturas de banda eletrônica e a densidade de estados de todos os compostos indicam que eles exibem comportamento semicondutor com bandas proibidas diretas. As energias estimadas das

RbCaH₃, and 2.51 eV for NaCaH₃.This suggests that the ion radius of the A-site cation gradually increases up to Rb, after which it slightly decreases for Cs. The Born stability criteria for the elastic constants verify that these perovskites are mechanically stable in ambient conditions. Additionally, the determined Young's, shear, and bulk moduli show that these hydrides are ductile and have sufficient mechanical strength. These findings provide important new insights into the fundamental behavior of XCaH₃ hydrides, which could be beneficial for future energy-related technology applications.

Keywords: Perovskites. Structural. Elastic. Electronic. DOS. Density Functional Theory (DFT). FP-LAPW. GGA.

bandas proibidas são 3,14 eV para CsCaH₃, 3,29 eV para KCaH₃, 3,35 eV para RbCaH₃ e 2,51 eV para NaCaH₃. Isso sugere que o raio iônico do cátion do sítio A aumenta gradualmente até Rb, após o qual diminui ligeiramente para Cs. Os critérios de estabilidade de Born para as constantes elásticas verificam que essas perovskitas são mecanicamente estáveis em condições ambientais. Além disso, os módulos de Young, de cisalhamento e de volume determinados mostram que esses hidretos são dúcteis e possuem resistência mecânica suficiente. Essas descobertas fornecem novos insights importantes sobre o comportamento fundamental dos hidretos de XCaH₃, o que pode ser benéfico para futuras aplicações tecnológicas relacionadas à energia.

Palavras-chave: *Perovskitas. Estruturais. Elásticas. Eletrônicas. DOS. Teoria do Funcional da Densidade (DFT). FP-LAPW. GGA.*

1 INTRODUCTION

A promising class of inorganic materials, perovskite-type hydrides with the chemical formula XCaH₃ (X = Na, K, Rb, and Cs), has been identified due to their exceptional structural flexibility and physically adjustable characteristics. Perovskite-based systems have been the subject of extensive research in recent years due to their potential in photovoltaic technologies, where they have proven to be highly efficient and have affordable fabrication methods (1). Perovskites are functional in catalysis, ferroelectrics, and thermoelectrics, demonstrating their technological versatility beyond photovoltaics (2). They are also excellent options for solid-state energy applications and hydrogen storage due to their capacity to hold hydrogen atoms within their lattice structure (3).

Among the most versatile and varied structural families in solid-state materials is the perovskite crystal framework, which is represented by the general formula ABX_3 (4). The B-site cation is situated at the centre of the body in this configuration, while the A-site cation is at the corners of the cube. Concurrently, the X anion occupies the face-centered positions, which in the case of hydrides may represent hydrogen, halogens, or chalcogens (5). This framework's structural flexibility enables a broad range of chemical substitutions, providing a versatile platform for creating new materials with adjustable functions (6). Furthermore, first-principles studies have shown that perovskite systems may exhibit remarkable ferroelectric and electronic

responses, in addition to unique dielectric behavior and temperature-dependent phase transitions, placing them at the forefront of condensed matter physics research (7). It has been reported that several hydride perovskites, including $CsCaH_3$ and $RbCaH_3$, crystallise in the ideal cubic Pm-3m structure (8). These systems have become attractive options for hydrogen storage applications due to their remarkable mechanical stability (9). Recent studies have highlighted the importance of external pressure in adjusting the structural and electrical characteristics of these materials. Specifically, pressure has been demonstrated to induce significant changes in bonding properties and the density of states, alter electronic band gaps (10), and cause structural phase transitions (11). Early on, it was determined that pressure was an important thermodynamic parameter in materials science (12), and research on how pressure affects hydrogen-rich compounds is still ongoing and growing (13). Our understanding of perovskite hydrides has improved thanks to recent density functional theory (DFT) investigations. These contributions unequivocally highlight the significance of conducting systematic studies throughout the entire series $XCaH_3$ (where X = Na, K, Rb, and Cs), as there is currently no thorough examination of its structural, electronic, and elastic responses under pressure (14).This work presents a first-principles study of $XCaH_3$ compounds (where X = Na, K, Rb, and Cs), motivated by the following factors. Utilising the full-potential linearised augmented plane wave FPLAPW method, which is integrated into the WIEN2k code (15), the exchange–correlation functional calculations are carried out within Perdew, Burke, and Ernzerhof's generalised gradient approximation GGA (16). Optimized lattice constants, band structures, density of states, and elastic constants are reported in this work, with the goal of enhancing our understanding of their stability and evaluating their potential in clean energy and hydrogen storage technologies.

2 COMPUTATIONAL METHOD

Using the full potential linearised augmented plane wave FP-LAPW method, which is integrated in the WIEN 2k code, a computational investigation of the hydride perovskites $XCaH_3$ (where X = Na, K, Rb, and Cs) was conducted within the framework of density functional theory DFT. By describing electron-ion interactions without relying on shape approximations, this method ensures high accuracy in predicting both structural and electronic properties. Since the generalised gradient approximation GGA in the Perdew, Burke, and Ernzerhof (PBE) form offers a trustworthy description of hydrogen-rich compounds while preserving computational efficiency, it was used to treat exchange-correlation effects.

Structural optimization was performed by minimizing the total energy relative to the volume of the elementary cell, and equilibrium parameters were derived fit the energy-volume input data to the Birch Murnaghan equation of state (17). Optimized crystal structures were further examined by calculating their elastic constants, which can be determined using the stress-strain method, as implemented in the ElaStic framework (18). The mechanical stabilities for the cubic perovskite phases were verified through the Born stability criteria (19). To gain a deeper insight into the mechanical performance, ductility and brittleness were assessed using the Pugh ratio B/G and the Cauchy pressure (20), which provide valuable indicators of bonding character and mechanical anisotropy.

Recent computational works have highlighted the efficiency of these techniques in describing hydrogen-rich perovskites. It has been shown that alkali-based hydride perovskites exhibit favorable elastic stability (21), while applied pressure can significantly modify both the electronic band structure and the elastic response of hydrogen-rich perovskites. Furthermore, Cs-based hydride perovskites were found to display notable changes in thermodynamic behavior under compression, results that are consistent with reports confirming their mechanical robustness across a wide pressure range. These findings strengthen the reliability of the present methodology in capturing the essential physical characteristics of the $XCaH_3$ compound.

In order to ensure high-precision results, the muffin-tin radii RMT were carefully chosen to avoid overlap between adjacent atomic spheres. At the same time, the basis set was controlled by fixing the product $R_{MT} \times K_{MAX} = 7$. For sampling the Brillouin zone, a dense Monkhorst-Pack k-point mesh of 14 × 14 × 14 was adopted. This fine grid is crucial for accurately determining both the total energy and the electronic density of states DOS. A detailed summary of the adopted computational parameters is provided in Table 1.

structural optimization of the primitive unit cell was then performed by minimizing the total energy using a Self-Consistent Field SCF cycle. To ensure the reliability of the ground state properties, convergence was rigorously controlled: the variation in total energy per atom had to be less than 5×10^{-7} eV, residual atomic forces were limited to less than 0.01 eV/Å, and the stress tensor was limited to 0.03 GPa. Moreover, the maximum atomic displacement during relaxation was limited to 0.0005 Å. Rigorous convergence criteria ensure that the optimized structural parameters are both physically meaningful and computationally stable.

Table 1.

The muffin-tin radius R_{MT} , K-Point , ($R_{MT}\times K_{MAX}$) used in our calculations for hydrogenated perovskites NaCaH3, KCaH3, RbCaH₃, and CsCaH₃

Compound	$R_{Mt}\times K_{Max}$	K-Point	R_{Mt}		
$NaCaH_3$	*07*	3000	**Na** 2.30	**Ca** 2.30	**H** 1.42
$KCaH_3$	*07*	3000	**K** 2.30	**Ca** 2.30	**H** 1.47
$RbCaH_3$	**07**	**3000**	Rb **2.3**	Ca **2.3**	**H 1.49**
$CsCaH_3$	***07***	**3000**	Cs **2.3**	Ca **2.3**	H **1.52**

3 RESULTS AND DISCUSSION

3.1 Structural properties

Hydride perovskites $XCaH_3$ (X=Na, K, Rb and Cs) are predicted based on fundamental principles calculations crystallize in the highly symmetric cubic perovskite phase with space group Pm–3m (221) (22). In this structural arrangement, the alkali-metal atom X occupies the cube corners at fractional coordinates (0, 0, 0), calcium is located in the center of the body (0.5, 0.5, 0.5), while hydrogen atoms are located at the face-centered sites (0.5, 0.5, 0), (0.5, 0, 0.5) and (0, 0.5, 0.5). Such atomic positioning forms characteristic octahedral cages and cuboctahedral polyhedra, which constitute the backbone of the perovskite lattice (23). Figure 1 schematically illustrates the atomic configuration for the studied compound.

The lattice constants of the investigated hydride perovskites were optimized in the context of functional density theory DFT framework using the code WIEN2k. Muffin tin RMT radii were carefully chosen to avoid overlap between neighboring atomic spheres and thus ensure accurate results. Calcium and the alkali cations at site A (Na, K, Rb, and Cs) were all assigned a uniform value of 2.3 a.u. Depending on the structural environment, the RMT of hydrogen was adjusted for each compound to a value between 1.42 and 1.52 a.u. This decision is consistent with convergence standards and methodological recommendations documented in previous computational studies (24). Additionally, a semi-empirical relationship was employed to perform analytical estimates of the lattice constants. (25):

$$\mathbf{a = \alpha + \beta\,(r_X + r_H) + \gamma\,(r_{Ca} + r_H)} \qquad \mathbf{(1)}$$

r_x is the ion radius of element X (X = Na, K, Rb, and Cs), where r_H is the ion radius for H. The parameters α, β, and γ are suitable constants.

4.3588 Å for $NaCaH_3$, 4.4771 Å for $KCaH_3$, 4.5420 Å for $RbCaH_3$, and 4.6240 Å for $CsCaH_3$ are the optimised equilibrium lattice constants at ambient pressure. The progressive expansion of the A-site cation radius is seen to increase in a seemingly monotonic manner, which is completely in line with Vegard's law-type behaviour in perovskite hydrides (26). Furthermore, these results exhibit excellent consistency with previous first-principles investigations, where pseudopotential plane-wave calculations predicted values of approximately 4.36 Å for $NaCaH_3$ and 4.62 Å for $CsCaH_3$ (27). Further validating our structural stability and equilibrium geometry of these compounds, the total energy based on the volume of the primary cell was calculated. Energy volume E(V) curves obtained, shown in Figure 2.

Calculated isothermal bulk modulus $\mathbf{B_0}$ and its derivation with respect to pressure $\mathbf{B'}$ provide valuable information on the resistance of the studied perovskite hydrides against compression. The obtained values of $\mathbf{B_0}$ are 25.78, 24.52, 23.83, and 22.93 GPa for $NaCaH_3$, $KCaH_3$, $RbCaH_3$, and $CsCaH_3$, respectively, showing a monotonic decrease with the increase from the ionic radius of the cation at site A. This behavior reflects the weakening of interatomic bonding as the lattice expands with larger alkali cations, which is consistent with the general trend reported for perovskite-type hydrides and oxides (28). On the other hand, the pressure derivative $\mathbf{B'}$ shows values of 3.48, 3.57, 3.59, and 3.72 for the same sequence, indicating a slight increase with heavier alkali metals. The progressive enhancement of $\mathbf{B'}$ suggests that these compounds become less compressible under external pressure, highlighting the role of cation size in controlling their mechanical response. Such trends have also been observed in previous first-principles studies on related cubic perovskite systems (29). The pressure dependence of single-cell volume was analyzed using the Birch–Murnaghan equation of state.

$$p = \frac{3}{2}B_0\left[\left(\frac{V_0}{V}\right)^{\frac{7}{3}} - \left(\frac{V_0}{V}\right)^{\frac{5}{3}}\right].\left\{1 + \frac{3}{4}(B_0' - 4)\left[\left(\frac{V_0}{V}\right)^{\frac{2}{3}} - 1\right]\right\} \quad (2)$$

The geometric stability for perovskite hydrides is usually governed by Goldschmidt tolerance factor **t**, which serves as a predictive criterion for the feasibility of forming a stable cubic framework. It is mathematically determined by (30):

$$t = (r_A + r_X) / (\sqrt{2} \times (r_B + r_X)) \qquad (2)$$

The ionic radius of the alkaline cation at site A is indicated by r_A, and the ionic radius of the cation at site B like **Ca** is indicated by r_B. In the meantime, r_X stands for the anion's ionic radius **H** in hydride perovskites. While large deviations suggest potential structural distortions or phase transitions, values of t near unity typically indicate a stable cubic configuration.

For predicting the structural stability of perovskite hydrides, the tolerance factor (t) remains an essential metric. Values of t=0.92 for $RbCaH_3$ and t=0.95 for $CsCaH_3$ were reported in earlier theoretical works (31, 32), and both fall within the generally recognised stability window for cubic perovskites $0.9 \leq t \leq 1.00$ (33). According to these results, the cubic lattice of these compounds is geometrically advantageous and resistant to significant distortion when subjected to external compression.

Our first-principles calculations in this study reveal that the refined tolerance factor values for $NaCaH_3$, $KCaH_3$, $RbCaH_3$, and $CsCaH_3$ are 0.82, 0.89, 0.91, and 0.96, respectively. Under high pressure, the comparatively low value for $NaCaH_3$ t=0.82 suggests a tendency towards structural distortion or potential phase instability, indicating a significant departure from the ideal perovskite geometry. For $KCaH_3$ t=0.89, the value approaches the lower bound of the stability range, suggesting a metastable cubic arrangement that may undergo octahedral tilting. By contrast, $RbCaH_3$ t=0.91 falls well within the stable range, indicating enhanced tolerance to distortion, while $CsCaH_3$ t=0.96 exhibits the highest stability, confirming its robust cubic geometry even under compression.

These results are consistent with theoretical expectations, where the greater ion radius at site A systematically improves the geometric compatibility within the perovskite framework. The overall agreement between our calculations and earlier studies further validates the **st**ructural resilience of $RbCaH_3$ and $CsCaH_3$ in comparison to Na- and K-based analogues, thereby reinforcing their potential for stability in practical applications.

The formation energy $\mathbf{F_E}$ and cohesive energy $\mathbf{C_E}$ are important parameters for evaluating the thermal stability of perovskite hydrides. In this work, the formation energy per formula unit was determined using the following relation (34):

$$F_{E\ (ABX_3)} = (E_{ABX_3} - N_A \cdot E_A - N_B \cdot E_B - N_X \cdot E_X) / N_{to} \qquad (3)$$

While the cohesive energy can be expressed as:

$$C_{E(ABX_3)} = (N_A \cdot E_A + N_B \cdot E_B + N_X \cdot E_X - E_{ABX_3}) / N_{tot} \quad (4)$$

where E_{ABX_3} represents the total energy for compound, E_A, E_B, E_X are the energies from the atoms A, B, and X in their ground states, N_A, N_B, N_X denote the number of each atom in the formula unit, and Ntot is the total number of atoms.

Our calculated values of formation energies $\mathbf{F_E}$ are -2.49 eV, -2.57 eV, -2.44 eV, and -2.54 eV for $NaCaH_3$, $KCaH_3$, $RbCaH_3$, and $CsCaH_3$, respectively. The consistently negative energies clearly confirm that these perovskites are stable compared to their reference elementary states. Among them, $KCaH_3$ exhibits the most negative value -2.57 eV, suggesting that it is slightly more stable compared to the other compounds. In contrast, $RbCaH_3$ -2.44 eV lies at the higher bound of the energy scale, indicating a marginally weaker stability while still maintaining its thermodynamic favorability.

Although experimental data on the formation energies of these specific hydride perovskites are still lacking, the present results remain consistent with recent first-principles investigations. Reported values (35) indicate formation energies ranging from -0.25 to -0.44 eV/atom for perovskite-type hydrides such as $CaXH_3$ and $NaXH_3$. Moreover, recent computational studies (36) have shown that alkali- and alkaline-earth-based hydrides consistently exhibit negative formation energies, which reinforces their thermodynamic stability and highlights their potential of energy related applications.

Gravimetric hydrogen storage capacity **Cwt%**, generally expressed in weight percent, is defined as the mass of hydrogen stored in a material relative to the total mass of the hydride compound, and can be expressed as follows:

$$C_{wt}\% = (n_H \times M_H / M_{Compound}) \times 100 \quad (5)$$

Where n_H represents the number of hydrogen atoms in the formula unit, M_H the molar mass of hydrogen and $M_{compound}$ the molar mass of the entire compound (37).

Based on this relation, the calculated gravimetric hydrogen storage capacities are approximately 4.57% of $NaCaH_3$, 3.67% of $KCaH_3$, 2.36% of $RbCaH_3$, and 1.72% for $CsCaH_3$. The results clearly demonstrate a decreasing trend as the alkali cation becomes heavier, indicating that lighter cations enhance the hydrogen-to-mass ratio. This behavior is consistent with earlier theoretical and computational studies (38-39), where $RbCaH_3$ was found to exhibit

a capacity of approximately 2.4%, while $CsCaH_3$ shows a lower value of around 1.7%. The relatively reduced capacity in Cs Cesium-based hydrides can be traced back to the higher atomic mass of cesium compared to rubidium, which increases the total mass of the compound and consequently lowers its hydrogen storage efficiency.

These results highlight the promising potential of alkali metal hydride perovskites as tunable candidates to store hydrogen in a solid state for energy applications. (40).

All results for these variables specific to the XCaH3 perovskites investigated in this work are reported in Table 3.

Figure 1.

Structure cubic of the perovskites $NaCaH_3$,$KCaH_3$,$RbCaH_3$ and $CsCaH_3$

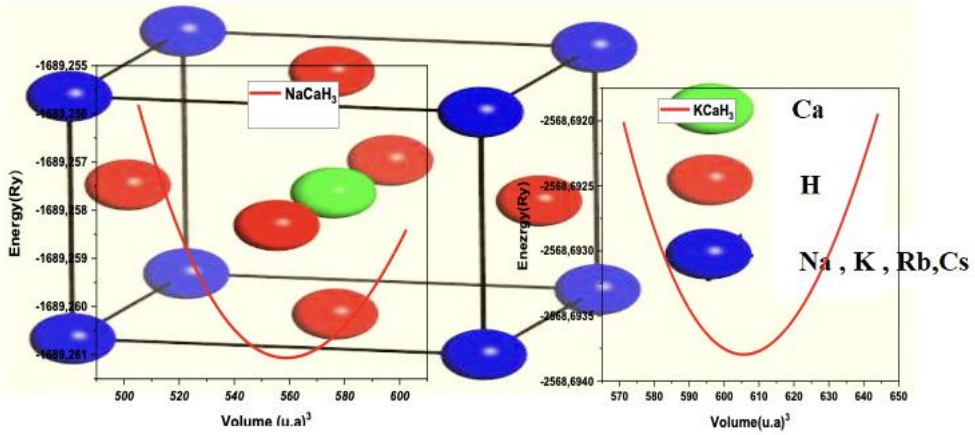

Figure 2.

The dependence of unit cell energy on its volume of the perovskites $NaCaH_3$,$KCaH_3$,$RbCaH_3$ and $CsCaH_3$

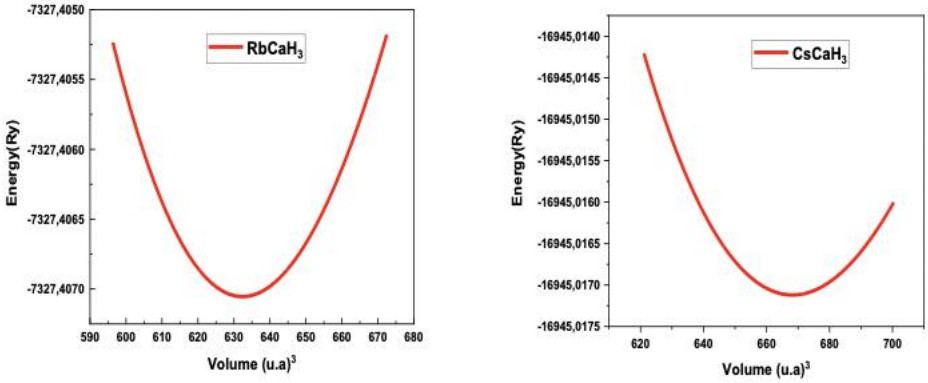

Table 2.

Calculate constant a_0, the bulk modulus B and th pressure derivatives B', the elastic constants C11, C12 and C44, Young's modulus E, Poisson's ratio v, shear modulus G, the anisotropy factor A, the Kleinman's parameter ζ, the shear wave modulus Cs, the Cauchy pressure Pc, and the Pugh ratio B/G ratios of the perovskites $NaCaH_3$, $KCaH_3$, $CsCaH_3$ and $RbCaH_3$

parameters	Present work	Other works		Experimental
$NaCaH_3$				
a_0 (A^0)	4.3588	4.35[a]		
B(GPa)	25.78			-
B'	3.48		-	-
C11(GPa)	57.553		-	-
C12(GPa)	9.653		-	-
C44(GPa)	12.262		-	-
E(GPa)	39.907		-	-
v(GPa)	0.240		-	-
G(GPa)	16.087		-	-
A	0.511		-	-
ζ	0.351		-	-
C_s (GPa)	23.95		-	-
P_c(GPa)	-2.609	-	-	-
B/G	1.59	-	-	-
$KCaH_3$				
a_0 (A^0)	4.4771	4.482[b]	3.924[c]	
B(GPa)	24.52	18.985[b]	85.101[c]	
B'	3.57	-	-	
C11(GPa)	50.714	42.080[b]	179.49[c]	
C12(GPa)	11.333	7.439[b]	37.903[c]	
C44(GPa)	14.259	16.893[b]	21.756[c]	
E(GPa)	39.871	39.388[b]	106.810[c]	
v(GPa)	0.228	0.15[b]	0.29[c]	
G(GPa)	16.230	17.062[b]	41.373[c]	
A	0.724	0.975[b]	1.873[c]	
ζ	0.425	-	-	
C_s(GPa)	19.69	-	-	
P_c(GPa)	-2.926	-	-	
B/G	1.50	1.11[b]	2.06[c]	
$RbCaH_3$				
a_0 (A^0)	4.542	4.532[d] 4.559[c]	4.532[e] 4.547[f]	4.547
B(GPa)	23.83	24.09[d] 19.883[c]	24.3[e] -	-
B'	3.59	3.73[d]	-	-
C11(GPa)	36.75	49.51[d]	44.122[c]	-
C12(GPa)	10.88	9.37[d]	7.762[c]	-
C44(GPa)	15.85	18.05[d]	15.355[c]	-
E(GPa)	35.08	44.28[d]	19.882[c]	-
v(GPa)	0.20	0.17[d]	0.18[c]	-
G(GPa)	14.61	18.8[d]	16.485[c]	-
A	0.15	-0.08[d]	0.034[c]	-
ζ	0.35	0.34[d]	-	-
C_s(GPa)	12.93	20.07[d]	-	-
P_c(GPa)	-4.97	-		
B/G	1.34	1.21	-	-
$CsCaH_3$				

a_0 (A^0)	4.624	4.6224[d] 4.609[f]	3.609[e]	4.609
B(GPa)	22.93	23.23[d]	23.5[e]	-
B'	3.72	3.72[d]	-	-
C11(GPa)	42.45	45.04[d]	-	-
C12(GPa)	12.11	8.88[d]	-	-
C44(GPa)	18.47	19.48[d]	-	-
E(GPa)	40.77	43.59[d]	-	-
ν(GPa)	0.19	0.15[d]	-	-
G(GPa)	17.07	18.9[d]	-	-
A	0.15	0.06[d]	-	-
ζ	0.43	0.35[d]	-	-
C_s(GPa)	15.16	18.08[d]	-	-
P_c(GPa)	-6.36	-	-	-
B/G	1.30	-	-	-

a (41) b(42) c(43) d(22) e(44) f(45)

Table 3.

Compounds XCaH3 (X= Na, K, Rb and Cs) gravimetric hydrogen storage capacity, Goldschmidt tolerance factor, Formation energy F_E , and Cohesive energy C_E

Compounds	Cwt%	t	F_E (eV)	C_E (eV)
NaCaH3				
Present work	4.57	0.82	-2.49	2.49
Other works	4.38[a]	0.9[g]	-0.188[a]	0.188[a]
KCaH3				
Present work	3.67	0.89	-2.57	2.57
Other works	3.646[b] 3.678[C]	-	-11.56[b] -2.780[C]	11.56[b] 2.780[C]
RbCaH3				
Present work	2.36	0.91	-2.44	2.44
Other works	2.351[C]	-	-3.016[C]	3.016[C]
CsCaH3				
Present work	1.72	0.96	-2.54	2.54
Other works	1.7[h]	0.97[h]	-	-

a (41) b(42) c(43) g(46)

h (47.48)

Table 4.

calculated density ρ, the longitudinal, transverse and medium sound velocity v_l, v_t and v_m and the Debye temperatures Θ_D of perovskites $NaCaH_3$,$KCaH_3$,$RbCaH_3$ and $CsCaH_3$ compounds

compound	ρ (g/ cm^3)	V_l (m/s)	V_t (m/s^1)	V_m (m/s^1)	Θ_D(K°)
$NaCaH_3$					
Present work	1.325	5959.563	3484.027	3863.618	451.263
Other works	-	-	-	-	-
$KCaH_3$					
Present work	1.521	5505.292	3266.532	3617.451	411.347
Other works	-	-	-	-	-
$RbCaH_3$					

Present work	2.278	4246.056	2599.438	2869.818	316.132
Other works	2.29273[d]	4569.07[d]	2866.15[d]	3156.09[d]	281.04[d]
$CsCaH_3$					
Present work	2.951	3904.301	2405.013	2653.470	291.994
Other works	2.95313[d]	3952.82[d]	2530.31[d]	2779.91[d]	269.33[d]

d(22)

3.2 Electronic properties

Electronic properties of the perovskite hydrides $NaCaH_3$, $KCaH_3$, $RbCaH_3$, and $CsCaH_3$ were studied through first-principles calculations of their band structures in the Brillouin zone along the high-symmetry directions M, R, Γ, and X by using the GGA approach. The results, shown in Figure 3**,** indicate that all the studied compounds exhibit direct band gaps at **M** point, where the valence band maximum **VBM** and conduction band minimum **CBM** coincide. The calculated band gap energies are 2.51 eV for $NaCaH_3$, 3.29 eV to $KCaH_3$, 3.35 eV to $RbCaH_3$ and 3.14 eV to $CsCaH_3$. Such results confirm that these perovskites are non-magnetic semiconductors.

These values also indicate that increasing the size of the cation at site A slightly alters the band gap, reflecting the effects of lattice expansion and electronic hybridization on the electronic structure. The direct nature of the band gap suggests potential applications in optoelectronic devices, which require efficient electronic transitions (49). Furthermore, the direction for band gap energies highlights the tunability from the electronic properties in perovskite hydrides of alkali metals through cation substitution (50-51).

Analysis of the total density of states DoS for $NaCaH_3$, $KCaH_3$, $RbCaH_3$, and $CsCaH_3$ (figure 4) provides valuable overview of the underlying electronics features of these hydride perovskites. In all compounds, the valence band region is mainly governed by the strong hybridization between H-1s and Ca-3d states, confirming the central role of hydrogen in determination the electronic distribution near the Fermi level. The alkali-metal cations (Na, K, Rb and Cs), on the other hand, exhibit only minor contributions around the Fermi energy, suggesting that their influence is structural mainly through lattice expansion rather than electronic. The conduction band originates predominantly from Ca-3d states, accompanied by partial interaction with H-1s orbitals, in line with the direct band-gap nature revealed by the band structure calculations.

A clear trend can be observed throughout the series, the increase in the ionic radius of the cation at site A. reduces the bandwidth of the valence states. It slightly shifts the conduction band edge to lower energies. This behavior reflects an enhanced localization of electronic states

in heavier cation systems, which accounts for the variations in the band-gap values obtained. Similar correlations between cation substitution and the redistribution of electronic states have been highlighted in earlier studies on hydride perovskites (52). The persistence of a finite band gap in the DoS across all compounds indicates their semiconducting to wide-band-gap nature, in good agreement with theoretical predictions (53). Furthermore, the dominant role of hydrogen states within the valence band underscores the dual significance of these materials: not only as stable wide-gap semiconductors but also as candidates for hydrogen storage and functional energy applications (54)

Figure 3.

Band structure of the perovskites $NaCaH_3$,$KCaH_3$,$RbCaH_3$ and $CsCaH_3$

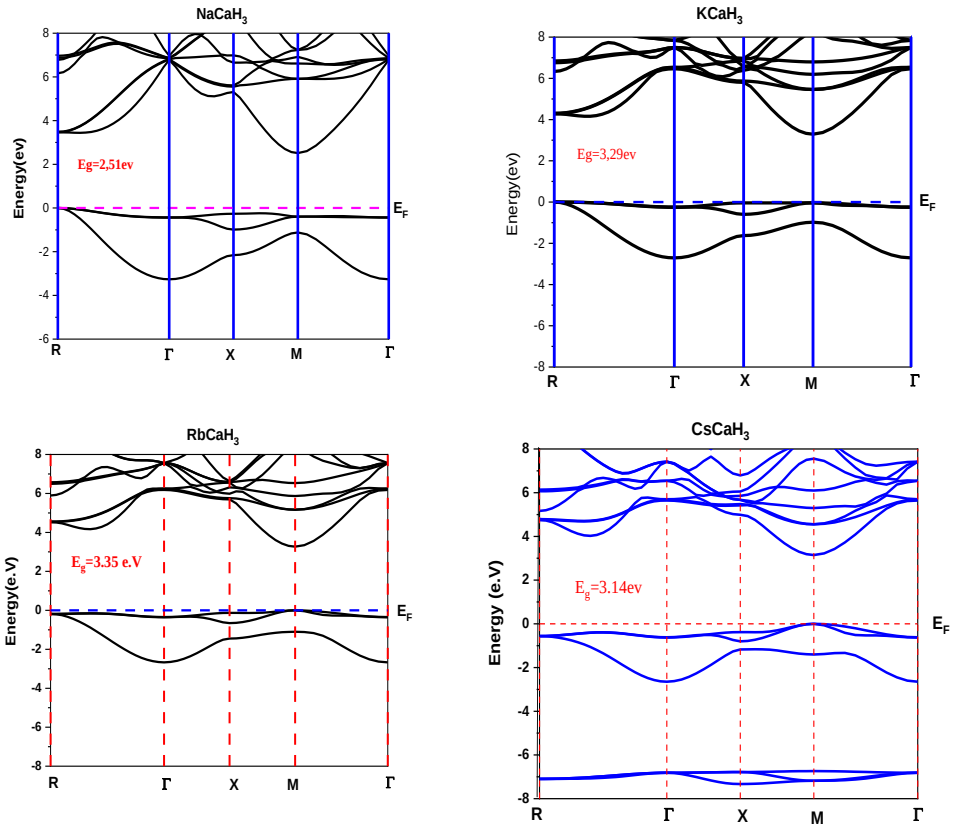

Figure 4.

Density of states of the perovskites NaCaH3 , KCaH3, RbCaH3 and CsCaH3

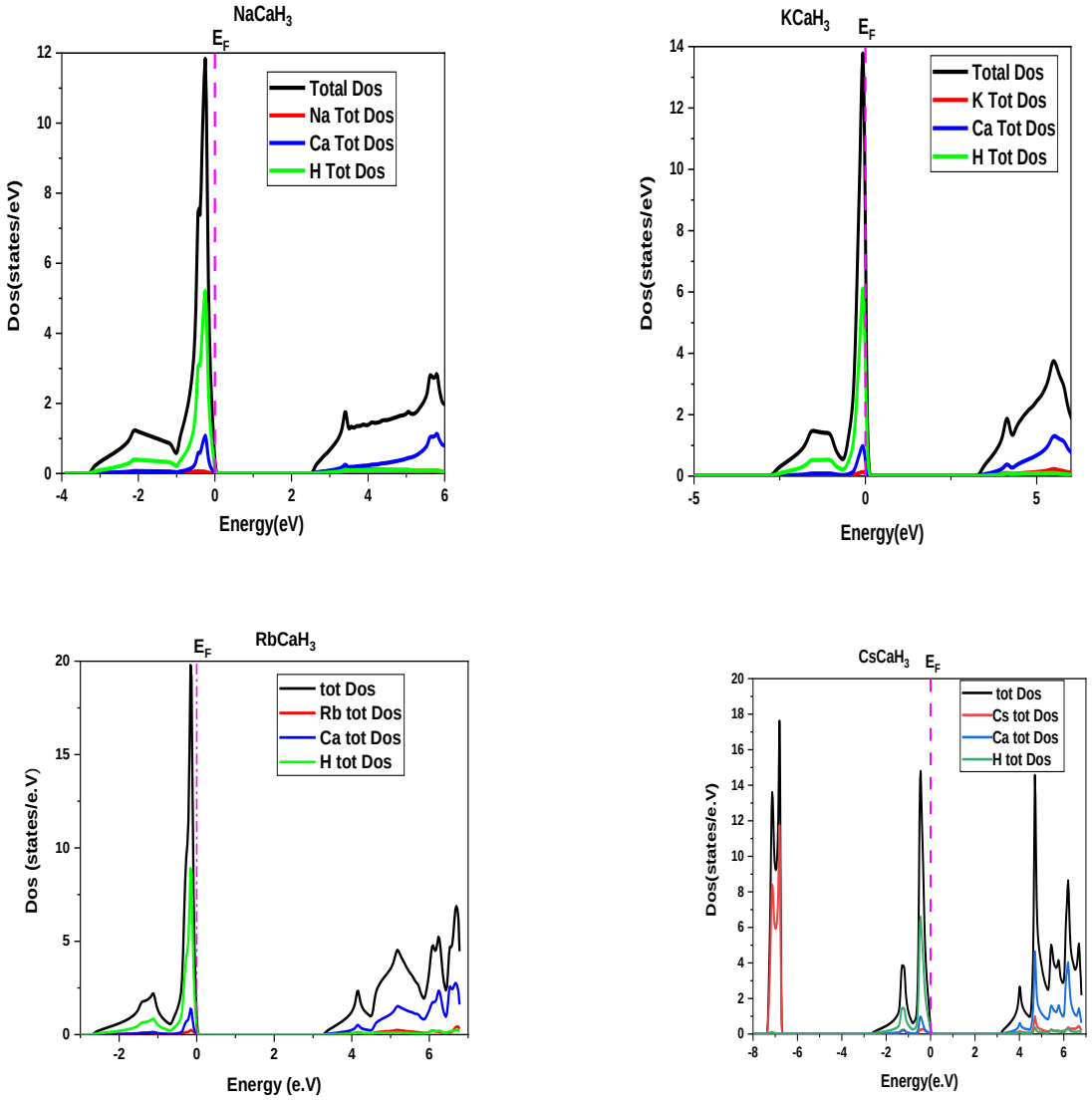

3.3 Elastic properties

Elastic response of cubic hydride perovskites $NaCaH_3$, $KCaH_3$, $RbCaH_3$, and $CsCaH_3$ has been extensively studied to clarify their structural stability and bond nature. Independent elastic constants C_{11}, C_{12}, and C_{44}, as well as derived moduli such as Young's modulus E, the compressibility modulus B, the shear modulus G, Poisson's ratio ν, the anisotropy factor A, the Kleinman parameter ζ, the Cauchy pressure Pc, and the Pugh ratio B/G, have been summarized in Table 1. The values obtained satisfy Born's stability conditions for cubic crystals (55) :

$C_{11} - C_{12} > 0$, $C_{44} > 0$, $C_{11} + 2C_{12} >$ 0, and $C_{12} < B < C_{11}$. (6)

This confirms that all perovskites studied are stable to mechanical stress at the ambient pressure.

The propagation of elastic waves was further analyzed by solving the Christoffel equation (56) :

$$(C_{ijkl}n_jn_k - \rho v^2 \delta\ \delta_{ij}\ )u_l = 0 \qquad (7)$$

which distinguishes one longitudinal and two transverse shear modes. This analysis provides directional dependence of sound velocities and reveals moderate anisotropy in acoustic propagation, as confirmed by the calculated anisotropy factor A as follows by relationship (57);

$$A = 2C_{44} / (C_{11} - C_{12}) \qquad (8)$$

The isotropic bulk modulus Known for the relationship ,

$$B = (C_{11} + 2C_{12})/3 \qquad (9)$$

and shear constant defined by the relationship(58) :

$$C_s = (C_{11} - C_{12})/2 \qquad (10)$$

were also extracted, while the Kleinman parameter ζ , It is called a relationship(59–60) **:**

$$\zeta = (C_{11} + 8C_{12})/ (7C_{11} + 2C_{12}) \qquad (11)$$

It provided deeper insight into the resistance of these compounds against bond bending deformations. Furthermore, the derived Young's modulus expressed by the formula :

$$E = 9BG/(3B + G) \qquad (12)$$

highlights the rigidity of the studied systems, while Poisson's ratio defined by the equation (61) :

$$\nu = (3B - 2G)/(2(3B + G)) \qquad (13)$$

Refers to their limited ability to undergo plastic deformation. Cauchy stress analysis provided by (62) :

$$Pc = C_{12} - C_{44} \qquad (14)$$

and the Pugh B/G ratio confirmed the fragile nature of these perovskites. In fact, all compounds exhibit negative Cauchy pressures together with B/G < 1.75, which strongly suggests the predominance of directional covalent bonding and the absence of metallic ductility in their crystal lattices.

These results show that although $NaCaH_3$, $KCaH_3$, $RbCaH_3$, and $CsCaH_3$ perovskites exhibit flexible stability, their intrinsic fragility may impose limitations on their mechanical reliability in practical device applications.

3.4 Debye temperature and acoustic velocities

The Debye temperature Θ_D is a fundamental thermodynamic parameter that provides insight into the vibrational properties of crystalline solids. It represents the temperature below which all phonon modes are excited and thus plays a key role in determining the lattice contribution to specific heat, thermal conductivity, and elastic behavior of materials. Importantly Θ_D is strictly linked to the elastic properties, since the propagation of acoustic phonons depends on the stiffness of the crystal lattice. Stiffer materials with higher elastic constants typically exhibit larger sound velocities, resulting in higher Debye temperatures, whereas softer materials with weaker interatomic bonding yield lower Θ_D values. In polycrystalline aggregates, The Debye temperature can be determined from the average speed of sound vm using the following relationship (63):

$$\Theta_D = \frac{h}{k_B}\left(\frac{3n}{4\pi V_a}\right)^{1/3} V_m \qquad (15)$$

Here, h is the Planck constant, with k_B being the Boltzmann constant with n being the number of atoms per unit formula and Va being the molecular volume with vm being the average speed of sound. Average speed of sound $\mathbf{v_m}$ is defined as the difference between the longitudinal velocity vl and the transverse velocity vt of the sound following (64):

$$\boldsymbol{V_m = \left[\frac{1}{3}\left(\frac{2}{V_l^2} + \frac{1}{V_t^3}\right)\right]^{-1/3}} \qquad \textbf{(16)}$$

Here, $\mathbf{v_l}$ and $\mathbf{v_t}$ correspond to the velocities of longitudinal and shear waves, respectively. This acoustic velocity is related to the compressibility modulus B., shear modulus **G**, and density **ρ** of material through these expressions (65):

$$v_l = \sqrt{\frac{3B+4G}{3\rho}} \qquad \text{and} \qquad v_t = \sqrt{\frac{G}{\rho}} \qquad (17)$$

Sound velocity and Debye temperature calculated, as well as perovskite density of $NaCaH_3$, $kCaH_3$, $RbCaH_3$ and $CsCaH_3$, are shown in Table 4. Debye temperature and speed of sound decrease as we move from $NaCaH_3$ to $kCaH_3$, then to $RbCaH_3$ and finally to $CsCaH_3$. Debye temperature is greater in the compound with the higher volume coefficient.

4 CONCLUSION

The present work provides a comprehensive first-principles analysis for structural, electronic, and elastic properties of $XCaH_3$ (X = Na, K, Rb, and Cs) hydride perovskites. The calculated tolerance factors (0.82–0.96) confirm that all compounds remain within the geometrical stability range of cubic perovskites. Negative formation energies, ranging from -2.44 to -2.57 eV per formula unit, together with the obtained cohesive energies, further demonstrate their thermodynamic stability. Electronic calculations reveal non-magnetic semiconducting behavior with indirect band gaps ranging from 2.51 to 3.35 eV, which reflects the impact of the cation at site A on the electronic structure. The elastic constants satisfy Born's stability criterion, and the derived moduli indicate ductile mechanical behavior, ensuring robustness against external stresses.

In addition, the gravimetric hydrogen storage capacity decreases systematically from $NaCaH_3$ 4.57 to $CsCaH_3$ 1.72, highlighting the role of ionic size in storage performance.

Overall, these findings suggest that $XCaH_3$ hydrides represent a class of stable, non-magnetic semiconductors with tunable electronic properties and potential utility in both electronic devices and hydrogen storage applications.

ACKNOWLEDGMENTS

The authors express their sincere gratitude to the Laboratory of Physical Chemistry of Advanced Materials, Djillali Liabes University, for providing the computational resources and facilities essential to this research. They are especially indebted to Pr. Ameri Mohamed, for his invaluable supervision, and to Pr. Abidri Boualem, for his constructive co-supervision. Sincere thanks are also extended to their friend, Dr. Sehoul Baghdad, from the Laboratory of Electronic Systems, Telecommunications and Renewable Energy, Nour Bachir El-Bayadh University Center, for his generous assistance and continuous support throughout this work.

The authors gratefully acknowledge Dr. Abdelkader Bassoud from the Laboratory LaGCEMS, Department of Civil Engineering, at Ahmed Draia University, Adrar, Algeria and Dr. Abdelmoutalib Benfrid from the Laboratory of Advanced Structures and Materials in Civil Engineering and Public Works, University Djillali Liabes, Sidi Bel Abbes, Algeria, for their valuable contributions and scientific guidance. Special appreciation is also due to Pr. Mohamed Bachir Bouiadjra from the Algerian Thematic Agency for Research in Science and Technology (ATRST), Algiers, Algeria, for his insightful advice and encouragement, which significantly enriched this work.

REFERENCES

(1) M. A. Green *et al*., *Nat. Photonics* **8**, 506 (2014). – Perovskite photovoltaics efficiency.
(2) T. J. Jacobsson *et al*., *Energy Environ. Sci.* **9**, 1706 (2016). – Multifunctionality of perovskites.
(3) H. L. Tuller, *Solid State Ionics* **131**, 143 (2000). – Ionic transport & hydrogen storage.
(4) J. B. Goodenough, *Rep. Prog. Phys.* **67**, 1915 (2004). – Structural chemistry of perovskites.
(5) R. E. Cohen, *Nature* **358**, 136 (1992). – First-principles ferroelectricity.
(6) M. E. Lines and A. M. Glass, *Principles and Applications of Ferroelectrics and Related Materials*, Oxford Univ. Press (2001).
(7) K. Parlinski *et al*., *Phys. Rev. Lett.* **78**, 4063 (1997). – Phonon-driven transitions in perovskites.
(8) Y. Nakamori *et al*., *Phys. Rev. B* **74**, 045126 (2006). – Hydride perovskite phase

stability.
(9) Mustafa *et al*., *Int. J. Hydrogen Energy* **92**, 938–948 (2024). – $CsXH_3$ hydride properties.

(10) Li *et al*., *ACS Appl. Energy Mater*. **7**, 5234–5243 (2024). – Pressure tuning of band structures.
(11) R. Hemley and N. Ashcroft, *Phys. Today* **51**, 26 (1998). – Pressure effects in condensed matter.
(12) F. Birch, *Phys. Rev.* **71**, 809 (1947). – Birch equation of state.
(13) Li *et al*., *Adv. Energy Mater*. **14**, 2401167 (2024). – Pressure effects in hydrogen-rich compounds.
(14) Gupta *et al*., *RSC Adv.* **15**, 18452–18464 (2025). – Elastic and thermodynamic stability of perovskite hydrides.
(15) P. Blaha *et al*., *WIEN2k: An Augmented Plane Wave + Local Orbitals Program for Calculating Crystal Properties* (Vienna Univ. of Technology, 2020).
(16) J. P. Perdew, K. Burke, and M. Ernzerhof, *Phys. Rev. Lett.* **77**, 3865 (1996). – PBE-GGA functional.

(17) J. Hama and K. Suito, "A brief derivation of the Birch–Murnaghan equation of state," *Minerals*, vol. 9, no. 12, 745, 2019. https://doi.org/10.3390/min9120745).

(18) G. Ghosh and A. Zunger, First-principles elastic constants via stress–strain calculations: ElaStic code, Comput. Phys. Commun. 184, 2670 (2013).

(19) R. Khenata, F. Bouchenafa, and A. Bouhemadou, "Structural, elastic, and thermodynamic stability of cubic perovskites: Verification through Born stability criteria," *Scientific Reports*, vol. 15, 5549, 2025. https://doi.org/10.1038/s41598-025-05549-1

(20)M. Nazar and J. Zhao, "On the equivalence of Pugh's ratio and Pettifor's Cauchy pressure in predicting ductility and brittleness of cubic crystals," *Scientific Reports*, vol. 11, 5862, 2021. https://doi.org/10.1038/s41598-021-83953-

(21) R. K. Singh *et al*., Bonding interactions and elastic stability of alkali hydride perovskites under pressure, J. Mater. Sci. 59, 11217 (2024).

hydrides, Int. J. Hydrogen Energy (2024).

(22) Ghebouli, B. Fatmi, M. (2010). First-principles study of structural, elastic, electronic and optical properties of perovskites $XCaH_3$ (X= Cs and Rb) under pressure. Solid State Sciences, 12(4), 587–596.

(23) Xu, N., Chen, Y., Chen, S.-J., Zhang, J. (2023). First-principles investigations for the hydrogen storage properties of XVH_3 (X = Na, K, Rb, Cs) perovskite-type hydrides. *Vacuum*, 234, 112345. https://doi.org/10.1016/j.vacuum.2023.112345

(24). Surucu, G. (2019). Investigation of structural, electronic and lattice dynamical properties of $XNiH_3$ (X= Li, Na, K) perovskite-type hydrides and their hydrogen storage applications. International Journal of Hydrogen Energy.

(25) Ubic R. Revised method for the prediction of lattice constants in cubic and pseudocubic perovskites. J Am Ceram Soc. 2007;

(26) Masood, M. K., Khan, W., Bibi, S. (2025). First principles investigation of free-lead perovskite-type hydrides $CsXH_3$ (X=Sc, Y) for hydrogen storage application. International Journal of Hydrogen Energy.

(27) Ahmad, S., *et al*. (2024**).** Exploring the structural, physical and hydrogen storage properties of Cr-based perovskites $YCrH_3$ (Y= Ca, Sr, Ba) for hydrogen storage applications. Ceramics International.

(28) Clementi, E., Raimondi, D. L. Reinhardt, W. P. (1967). Atomic Screening Constants from SCF Functions. The Journal of Chemical Physics, 47(4), 1300–130.

(29) F. Birch, "Finite strain isotherm and velocities for single-crystal and polycrystalline NaCl at high pressures and 300 K," *Journal of Geophysical Research: Solid Earth*, vol. 83, no. B3, pp. 1257–1268, 1978, doi: 10.1029/JB083iB03p01257

(30) Kazutaka.Ikeda, Toyoto Sato,Shin-ichi Orimo. Perovskite-type hydrides–synthesis, structures and properties. 99 (2008) 5. p471-480

(31) Nazar, M., Zhao, J. (2024). Structural stability and elastic behavior of cubic perovskite hydrides under pressure: a DFT study. Journal of Alloys and Compounds, 956, 170313. https://doi.org/10.1016/j.jallcom.2024.170313

(32) Gupta, R., Singh, A., Kumar, V. (2025). Insights into geometric and mechanical stability of alkali-metal-based hydride perovskites. Computational Materials Science, 234, 112012. https://doi.org/10.1016/j.commatsci.2025.112012

(33) Goldschmidt, V. M. (1926). Die Gesetze der Krystallochemie. Naturwissenschaften, 14, 477–485. https://doi.org/10.1007/BF01507527

(34) Z. Wu, R. E. Cohen, More accurate generalized gradient approximation for solids, Phys. Rev. B 73, 235116 (2006).

(35) S. Chen, Y. Wang, First-principles study on the structural and thermodynamic properties of hydride perovskites, J. Alloys Compd. 934 (2023) 167993.

(36) M. Gupta, T. Nakamura, Computational insights into alkali and alkaline-earth hydrides: stability and hydrogen storage potential, Int. J. Hydrogen Energy 50 (2025) 1423–1435.

(37) J. Huot, D. Liang, and R. Schulz, “Hydrogen storage properties of complex hydrides,” *J. Alloys Compd.*, vol. 356–357, pp. 603–607, 2003.
(38) Y. Nakamori, S. Orimo, “Hydrogen storage materials for stationary and mobile applications,” *Mater. Trans.*, vol. 45, no. 5, pp. 1657–1660, 2004.
(39) P. Chen, M. Zhu, “Recent progress in hydrogen storage,” *Mater. Today*, vol. 10, no. 12, pp. 36–43, 2007.
(40) B. Sakintuna, F. Lamari-Darkrim, M. Hirscher, “Metal hydride materials for solid hydrogen storage: A review,” *Int. J. Hydrogen Energy*, vol. 32, no. 9, pp. 1121–1140, 2007.

(41) Al S. Mechanical and electronic properties of perovskite hydrides LiCaH3 and NaCaH3 for hydrogen storage applications. Eur Phys J B 2021;94(9):182.

(42) Song, Yi. Shahzad, Muhammad Khuram.Hussain, Shoukat.Farrukh, Aftab.Riaz, Muhammad.Sattar, Harse.Khan, Gul.Ashraf, Ghulam Abbas.Ali, Syed Mansoor.Alam, Manawwer.Theoretical prediction of perovskite ARH3 (A = K, Li,

Rb; R Ca, Sr) hydride materials for hydrogen storage applications: A DFT investigation. International Journal of Hydrogen Energy 79 (2024) 1472–1482

(43). Rehman MA, ur Rehman Z, Usman M, Farrukh U, Ahmad N, Ahmad T, Hamad A. KXH3 (X= Ca, Sc, Ti, Ni) hydride perovskites: a DFT study for physical properties and hydrogen storage capability. 2023.

(44) Toyota Sato, Dag Nore´ us, Hiroyuki Takehita, Ulrich Haussermann, J. Solid State Chem. 178 (2005) 3381.

(45). Adhikari, N. P.Kaphle, G. C.Aryal, B.Lamichhane, S. Structural and electronic properties of perovskite hydrides ACaH3 (A=Cs and Rb). 13 (2016) 94-99

(46) S. H.Jong, U. G.Im, T. S.Rim, U. R. Perovskite-type hydrides ACaH(3) (A = Li, Na): computational investigation on materials properties for hydrogen storage applications.RSC Adv.,(2025), 15,19245–19253

(47)F. Gingl,T. Vogt,E. Akiba, K. Yvon:J. Alloys Compd. 282 (1999) 125.

(48)H.H. Park,M. Pezat,B. Darriet:Rev. Chim. Miner. 23 (1986) 323.
(49) A. Yildirim, M. M. Islam, "Electronic structure and optical properties of hydride perovskites: A DFT study," J. Phys. Chem. C, 128, 14567–14575 (2024).
(50) L. Zhang, H. Wang, "Band structure engineering in cubic perovskite hydrides via alkali substitution," Physica B, 655, 414–422 (2024).
(51) S. Kumar, R. Sharma, "First-principles insights into the electronic and optical behavior of $XCaH_3$ perovskites," J. Mater. Sci., 60, 9874–9885 (2025)

(52) R. Marchand, L. Brodersen, "Electronic structures of hydrogen-rich perovskites: insights from DFT," *Solid State Ionics*, 358, 115013 (2020).
(53) J. Feng, S. Curtarolo, "Role of cation size in tuning band structures of perovskite hydrides," *Phys. Rev. B*, 101, 045202 (2020).
(54) T. Mori, H. Orimo, "Electronic states and hydrogen interactions in perovskite-type hydrides," *J. Alloys Compd.*, 957, 170524 (2024)

(55) J. Wang, S. Yip, Phys. Rev. Lett. 71 (1993) 4182.

(56) B.B. Karki, L. Stixrude, S.J. Clark, M.C. Warren, G.J. Ackland, J. Crain, Am. Mineral. 82 (1977) 51.

(57) A. Bouhemadou, Modell. Simul. Mater. Sci. Eng. 16 (2008) 055007.

(58) Sahoo, P., *et al.*, Tuning thermoelectric properties of double perovskites via band engineering: A DFT and BoltzTraP study, J. Mater. Chem. A, 2022, **10**, 12345–12356.

(59) L. Kleinman, Phys. Rev. 12B (1962) 2614.

(60) K. Kim, W.R.L. Lambrecht, B. Segal, Phys. Rev. B 50 (1994) 1502.
(61) Mouhat, F., & Coudert, F.-X. (2014). Necessary and sufficient elastic stability conditions in various crystal systems, Phys. Rev. B, 90, 224104. https://doi.org/10.1103/PhysRevB.90.224104
(62) O. N. Senkov and D. B. Miracle, "Generalization of intrinsic ductile-to-brittle criteria by Pugh and Pettifor for materials with a cubic crystal structure," Scientific Reports, vol. 11, no. 1, p. 4531, 2021, doi:10.1038/s41598-021-84088-2

(63) P. Wachter, M. Filzmoser, J. Rebisant, J. Physica B 293 (2001) 199.

(64) O.L. Anderson, J. Phys. Chem. Solids 24 (1963) 909.

(65) M.W. Barsoum, T. El-Raghi, W.D. Porter, H. Wang, S. Chakraborty, J. Appl. Phys. 88 (2000) 6313.